Journal of Applied Fluid Mechanics, Vol. 16, No. 5, pp. 920-931, 2023.
Available online at www.jafmonline.net, ISSN 1735-3572, EISSN 1735-3645.
https://doi.org/10.47176/jafm.16.05.1600

Influence of Bionic Waveform Leading Edge Blade on Drag Reduction Characteristics of Mixed Pump

W. Han[1,2], J. Zhang[1†], M. Z. Xiao[1], X. N. Ma[1], Z. Qu[1] and F. Yin[3] and Q. Sun[3]

[1] *College of Energy and Power Engineering, Lanzhou University of technology, Lanzhou, Gansu, 730050, China*
[2] *Key Laboratory of Fluid machinery and Systems, Lanzhou, Gansu, 730050, China.*
[3] *CNOOC Research Institute Co., Ltd., Beijing, 100028, China*

†*Corresponding Author Email: 18419062369@163.com*

(Received October 5, 2022; accepted January 2, 2023)

ABSTRACT

Because the helical axial flow gas-liquid mixing pump has the great advantage of conveying gas-liquid two-phase mixed medium, it has become the main core equipment for deep-sea oil and natural gas exploitation. The gas phase aggregation and bubble movement trajectory in the impeller channel have been widely studied, but the increase of medium flow resistance caused by flow separation has not been deeply discussed. Combined with the Euler multiphase flow model and the SST k-ω turbulence model, the numerical calculation of the helical axial flow gas-liquid mixed pump is carried out. Under design flow conditions Q = 100 m^3/h, head H = 30 m, speed n = 4500 r/min, specific speed n_s =213.6 r/min, and under different inlet gas content conditions, the influence of the bionic waveform leading edge blade on drag reduction characteristics of the helical axial flow gas-liquid mixed pump was investigated. By designing the blade with a leading-edge structure with different heights and pitches, the separation of the mixed medium and the suction surface is effectively suppressed, and the flow resistance of the medium in the 1/10 area of the inlet end of the blade is reduced. The results show that when the height A is 0.25%L and the pitch λ is 12.5%h, the maximum drag reduction rate in this region is 52.6%, the maximum increase in efficiency of the mixed pump is 2.2%, and the maximum increase in head is 4.8%. This study can provide technical support for flow drag reduction in gas-liquid mixed pump.

Keywords: Helical axial flow gas-liquid mixing pump; Waveform edge; Separation; Drag reduction; Bionic waveform.

NOMENCLATURE

A	height	Q	design flow
D	impeller diameter	Z	blade number
H	head	β_1	inlet placement angle
h	blade height	β_2	outlet placement angle
L	chord length	γ	hub half cone angle
n	speed	λ	pitch

1. INTRODUCTION

With the rapid economic growth in recent years, the consumption of oil and natural gas is increasing day by day. All countries have faced with the shortage of oil resources and the exploration of new oil resources has become very difficult. Therefore, the development of oil and natural gas resources has gradually moved from the mainland to the deep sea area (Li 2019; Pan *et al.* 2016). The composition of deep-sea oil is complex, and sustainable and efficient transportation is a costly and difficult process. In recent years, the government of different countries have invested a lot of resources in the research of mixed pump technology, which has become an ideal equipment for transferring oil and has solved some difficulties of oil transferring (Liu *et al.* 2019; Rabha *et al.* 2015). Compared with traditional mining technology, the gas-liquid mixed pump technology has low investment cost and convenient management (Suh *et al.* 2017; Yu *et al.* 2004). Due to the small placement angle (angle between the tangent line and

the circumferential direction of the blade airfoil bone line at the inlet) of the impeller blades of the helical axial-flow gas-liquid mixed pump, when the gas-liquid two-phase mixed medium enters the impeller, it will be impacted by the leading edge of the blade inlet and cause a flow detachment phenomenon. It also causes the flow resistance of the mixed medium to increase, resulting in a decrease in the performance of the mixed pump (Ma *et al.* 2021; Zhao *et al.* 2022). Since the angle of incidence is dependent on the relative flow, the phenomenon of flow separation is probably related to the small thickness of the blade. Therefore, this paper proposes the modification of the leading edge of the mixed pump blade to achieve significant drag reduction.

At present, many scholars have proposed flow control technology, the role of which is to change the position of medium transition, turbulence intensity, secondary backflow, and reduce resistance. In practical engineering, the application of this technology includes bionic waveform leading edge blades, vortex generators on the surface of aircraft wings, guide grooves on the surface of blades, ball sockets on the surface of golf balls, etc. The waveform leading edge blade is a bionic blade originated from biologists' research on the shape of humpback whale fins. Studies have shown that the fin profile of humpback whales has greater lift and less drag than a control model with a smooth leading edge (Guo *et al.* 2019; Zhang and Li 2020). Based on the profile of the NACA 0021 airfoil with wavy leading edge modification, Fonseca et al. studied the flow around the airfoil at Reynolds number 3×10^6 numerically. The research results showed that the maximum lift coefficient and the stall angle of the wave leading edge increase and the drag coefficient of the wave leading edge airfoil is higher than that of the straight leading edge airfoil, when the angle of attack is close to the stall angle (Fonseca *et al.* 2020). Zhao et al performed dynamic modal decomposition (DMD) analysis on smooth airfoils and airfoils with wavy leading edge structures at Re = 1.2×10^5 under stall condition. By analyzing the counterflow profile near the laminar separation bubble (LSB), it was found that the improved aerodynamics at the crest of the wave-like structure stems from the strong flow-direction vortex caused by the leading edge protrusion (Zhao *et al.* 2020). Wu et al. investigated the effects of bionic blades on aerodynamic performance, flow field and sound field of centrifugal fans. The results showed that the bionic structure inhibits the flow separation of blade suction surface, improves the total pressure and efficiency of the centrifugal fan, and changes the flow field and vortex shedding structure of the main airfoil (*Chen et al.* 2021; Wu *et al.* 2021).

With the help of the existing research studies, along with the principle of bionics, the research results of the fin shape of the humpback whale are used to design the leading edge of the mixed pump blade, and the external characteristics and internal flow of the modified mixed pump are analyzed. The characteristics are analyzed to provide theoretical support for suppressing the flow separation caused by the impact of the leading edge of the mixed pump blade and reducing the resistance of the mixed medium.

2. RESEARCH OBJECT DESIGN AND GRID INDEPENDENCE TEST

2.1 Research Object Design

The moving medium in this paper is a gas-liquid two-phase mixed medium, and the single-stage screw axial flow gas-liquid mixed transport pump is used as the research object. The pump design flow Q = 100 m^3/h, head H = 30 m, speed n = 4500 r/min, specific speed n_s = 213.6 r/min, impeller diameter D = 150 mm, blade number Z = 4, hub half cone angle γ = 6°, blade inlet placement angle β_1 = 10°, the blade outlet placement angle β_2 = 10°, and the axial length of the impeller e = 55 mm are considered in numerical simulation. Fig.1 shows the computational domain model of the mixed pump.

2.2 Waveform Leading Edge Scheme Determination

The convex structure of the humpback whale is simplified, and the convex model of the sinusoidal structure is selected as an alternative to study the mechanism. The schematic diagram of the waveform model of the sinusoidal structure is shown in Fig. 2, where the horizontal axis represents the waveform pitch λ and the vertical axis represents the waveform height A (Wang 2014). The ratio of the chord length L (L = 200 mm) of the impeller at a position of 0.5 times the blade height (h = 20 mm) to the radial height of the blade leading edge is about 10, which is much larger than the ratio of the airfoil chord length of the humpback whale flipper profile to its leading edge. So the key parameters of the sine curve are reduced within the original value range, and the relationship between the height A and pitch λ and the chord length of 0.5 times blade height position is determined as: 0.125% L < A < 1.2% L, 10% h < λ < 50% h. In this study, five groups of parameters are mainly drawn up, in which the height A is 2mm, 1 mm, 0.5 mm, and 0.25 mm and the pitch λ is 5 mm and 2.5 mm. The final parameter combination is shown in table 1.

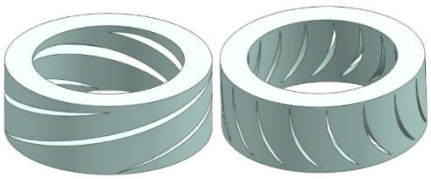

Fig. 1. Impeller and guide vane computational domain model of mixed pump.

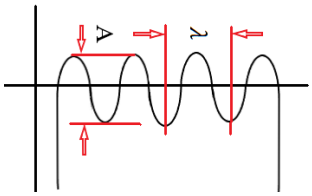

Fig. 2. Schematic diagram of height *A* and pitch *λ* of the waveform structure.

Table 1 Geometric parameters of the bionic waveform leading edge structure

Scheme	Height (mm)	Pitch (mm)
*A*2*λ*5	2	5
*A*1*λ*5	1	5
*A*1*λ*2.5	1	2.5
*A*0.5*λ*2.5	0.5	2.5
*A*0.25*λ*2.5	0.25	2.5

2.3 Grid Independence Test

The meshing software ICEM CFD 17.0 is used to mesh the computational domain, as shown in Fig. 1. It is noted that the more meshes are generated, the more accuracy is achieved. But at the same time, the load on the computer increases and as a result, the computing resources are wasted. Therefore, considering the external characteristic-efficiency of the design flow condition of the mixed pump as the evaluation measure, the grid independence test is carried out on the calculation model domain. As shown in Figure 3, when the number of grids is more than 6.25 million, the variation of mixed pump efficiency is stable. In order to save the computing resources, the grid number is finally set at 6.25 million.

Figure 4 shows an enlarged view of the computational domain grid of the modified mixed pump and the grid of the leading edge blade of the *A*2*λ*5 waveform.

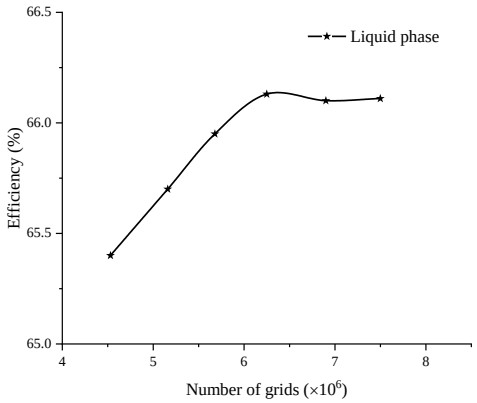

Fig. 3. Grid independence test.

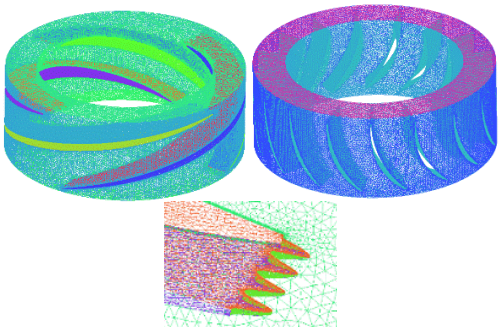

Fig. 4. Impeller and guide vane computational domain grid and waveform leading edge grid of scheme *A*2*λ*5.

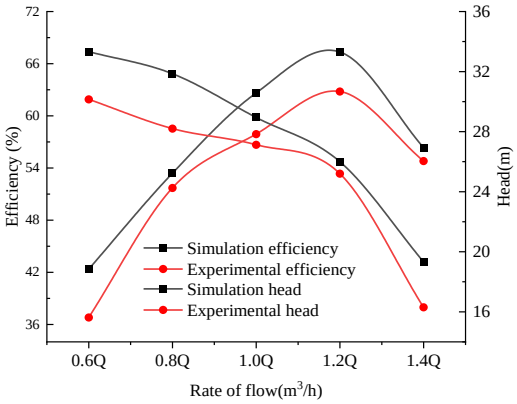

Fig. 5. Comparison of external characteristics between numerical simulation and experimental.

2.4 Numerical Method Validation

In order to verify the accuracy of the numerical method, this paper is based on the gas-liquid two-phase flow experimental bench. The external characteristics of the mixed pump at IGVF = 50%, five flow conditions with flow rates of 0.6*Q*, 0.8*Q*, 1.0*Q*, 1.2*Q*, 1.4*Q* are conducted in the experiment , where Q =100 m^3/h. The experiment results are compared with the numerical simulation results of external characteristics under the same working conditions, as shown in Fig. 5. It can be seen from Fig. 5 that the numerical simulation results are in good agreement with the experimental results. When the IGVF is 50% and the design flow rate Q = 100 m^3/h, the numerical simulation efficiency of the mixed pump is 65.7% and the head is 31m, and the experimental efficiency of the mixed pump under the same working conditions is 60.5% and the head is 29m. The error between the numerical simulation results and the experimental results in the design flow conditions is in the range of 8%, which is in a reasonable range and indicates the reliability and accuracy of the selected numerical calculation method (Li 2020).

3. FLOW CONTROL EQUATIONS AND BOUNDARY CONDITIONS

3.1 Flow Control Equations

The moving medium of the mixed pump is a gas-liquid two-phase mixed medium, and the flow state of the medium in the flow channel is complicated, but from the macroscopic dimension, it still obeys three conservation laws: mass conservation, energy conservation and momentum conservation (Li et al. 2021; Li et al. 2022). For the internal flow problem of the mixed pump, it can be regarded as the solution of a viscous incompressible flow problem without heat exchange. The equations of motion for a viscous incompressible fluid are as follows (Wang 2020):

Continuity Equation:

$$\frac{\partial}{\partial t}(\alpha_k \rho_k)+\nabla\cdot(\alpha_k \rho_k U_k)=0 \tag{1}$$

Momentum Equation：

$$\frac{\partial}{\partial t}(\alpha_k \rho_k U_k)+\nabla \cdot (\alpha_k \rho_k U_k U_k - \alpha_k \tau_k) = -\alpha_k \nabla p + M_k + \alpha_k \rho_k f_k \quad (2)$$

Where k represents different phases, when $k = l$, it represents the liquid phase, and when $k = g$, it represents the gas phase. α_l and α_g are the dimensionless numbers of the volume fractions of the liquid and gas phases in the mixed medium, respectively; ρ_l and ρ_g are the densities of the liquid and gas phases; U_l and U_g are the flow velocities of the liquid and gas phases; p is the pressure; f_l and f_g are the masses of the liquid and gas phases; M_l and M_g are the surface tensions of the liquid and gas phases.

3.2 Boundary Conditions

Based on ANSYS Fluent 17.0 software, the three-dimensional numerical simulation of the flow field of the mixed transport pump was carried out, and the steady-state characteristics of the flow field in the cascade channel were simulated by the Navier-Stokes equations. Subsequently, the governing equations of the flow were discretized and solved by the SIMPLE algorithm. The Euler multiphase flow model and the *SST k-ω* turbulence model are used for fluid flow simulation. The velocity inlet is selected for the inlet, the pressure outlet is selected for the outlet, the no slip wall condition is selected for the flow wall, the impeller calculation domain is set to the rotating domain, and the rest of the computational domain are set as static domains. The conveying medium of the mixing pump is two-phase flow, the main phase is liquid phase, the secondary phase is gas phase, the bubble diameter is 0.1mm (Zhang et al. 2016; Zhou 2021), and the convergence accuracy is set to 10^{-5}.

4. ANALYSIS OF CALCULATION RESULTS

4.1 Vortex System Analysis of Bionic Waveform Leading Edge Blade

The energy dissipation of the mixed medium can be measured by the vorticity intensity. The greater the vorticity intensity, the more energy dissipation is generated (Wu 1986). Fig. 6 shows the vorticity intensity nephogram of the blade under different schemes under the design flow condition (Q = 100 m^3/h) and the IGVF is 40%. The vortex degree of the separation zone is judged by the eigenvalues of the Q criterion. The Q-Criterion Level is chosen as 0.01 to process the blade leading edge vortex system, and the vortex system is colored with liquid phase velocity. It can be seen from a) that the vortex system (red area) extending along the flow direction appears on the suction front edge of the original model blade and the area with higher speed includes the larger extension region of the vortex system. From b), c), d) and e), it can be seen that although the speed of the blade near the rim is still significantly greater than that at the hub, the vortex system at this time does not appear to extend in the direction of flow, and mainly accumulates in the valley area. This is because under the influence of the leading edge of the waveform, when the mixed medium flows through the peak region of the leading edge of the waveform, the initial pressure gradient distribution changes along the flow direction. So the vortex system no longer expands along the flow direction, but accumulates in the low-pressure to reduce the energy loss of mixed medium. From f), it can be seen that the vortex system extends along the flow direction, that is the waveform leading edge under

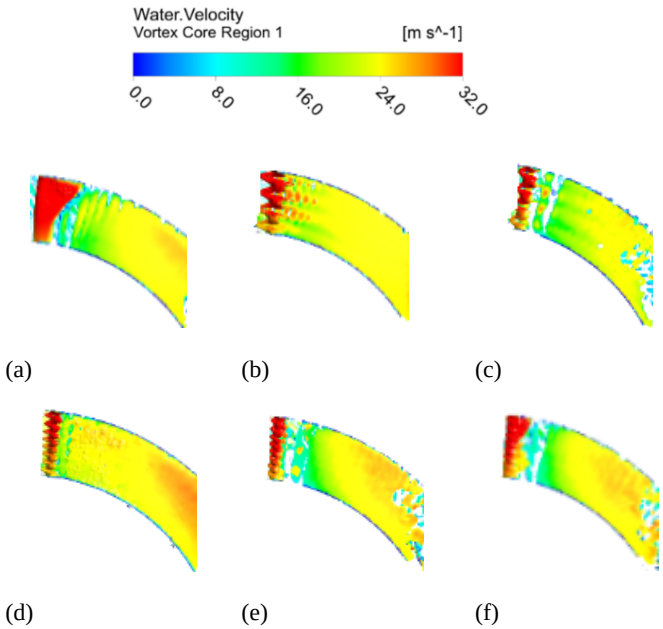

Fig. 6. Vorticity intensity cloud map of different schemes: a) original model; b) *A*2λ5; c) *A*1λ5; d) *A*1λ2.5; e) *A*0.5λ2.5; f) *A*0.25λ2.5.

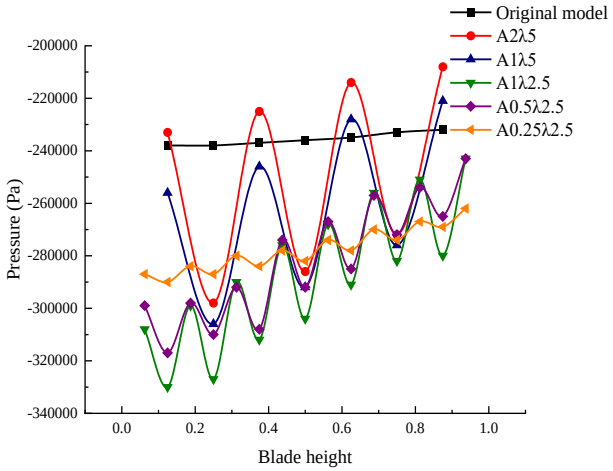

Fig. 7. Pressure changes in the crest and trough areas in the direction of blade height under different scenarios.

Table 2 Relevant parameters of the fitting function between pressure and blade height.

Scheme	a_0	a_1	b_1	a_2	b_2	a_3	b_3	a_4	b_4	ω
$A2\lambda5$	-253700	7833	-8696	5202	4008	-22290	24500			7.9
$A1\lambda5$	-265300	10120	-11270	5536	3240	-15410	22420			7.8
$A1\lambda2.5$	-286300	4667	-24310	6458	-9217	7068	-4173	6387	-4062	
$A0.5\lambda2.5$	-281200	5570	-22820	6003	-8004	4207	-4621	6187	-3476	
$A0.25\lambda2.5$	-287000	-351	-8194	-1080	-4014	-477	-2361	-648	-1343	
Scheme	a_5	b_5	a_6	b_6	a_7	b_7	a_8	b_8	ω	
$A1\lambda2.5$	7079	-2369	6490	-1330	6635	48.86	9915	-5303	6.37	
$A0.5\lambda2.5$	3841	-963	3300	-690	5359	1127	-5470	-4336	6.42	
$A0.25\lambda2.5$	-371	-877	-62	-281	537	-52	-2161	-1022	6.39	

this scheme cannot effectively restrain the separation vortex from extending to the flow direction. It shows that when the pitch λ is equal to 12.5% *h*, the effect of suppressing the extension of the vortex system along the flow direction decreases as the height decreases.

Figure 7 shows the relative pressure changes in the peak and trough areas of the original model in the direction of the blade height using different schemes under design flow conditions. The IGVF is 40%, taking the trough horizontal line as the benchmark. The pressure in the original model in the figure increases gradually from the impeller hub to the rim, confirming that the pressure is higher in the regions of higher velocities. The relative pressure curve of a blade with a bionic waveform leading edge has the characteristics of high crest and low trough, and the pressure gradient of the crest and trough decreases with the decrease of wave height and pitch. Along with the vorticity intensity nephogram in Fig. 6, when there is a pressure gradient along the blade height, it is beneficial to restrain the vortex system from extending along the flow direction. An excessively large pressure gradient enhances the vorticity intensity in the low-pressure region of the trough, while a pressure gradient that is too small is not enough to destroy the original vortex system, so it can't achieve the effect of restraining the vortex system from extending along the flow direction. Overall, the relative pressure (y) in the crest and trough regions of the blade with different modification schemes has a Fourier series relationship with the blade height (x). As the height and pitch decrease, the order of the Fourier seriesincreases. The fitting function is as follows:

$$y = ax^2 + bx + c \tag{3}$$

a=7619.04; b=952.38; c=-238428.57.

Different modification schemes :

$$y = a_0 + \sum_{n=1}^{\infty}[a_n \cos(n\omega x) + b_n \sin(n\omega x) \tag{4}$$

4.2 Resistance Characteristic Analysis

After the mixed medium enters the impeller, its flow direction changes from axial to peripheral with the rotation of the blades, and as a result, it is separated at the leading edge of the blade. Because the gas-liquid

mixed medium of the mixed pump is a fluid with high Reynolds number, the resistance is mainly caused the frictional stress of the mixed medium on the wall, that is the shear stress on the wall by the viscosity of the medium and the Reynolds stress in the turbulent state (Gu *et al.* 2015; Wu *et al.* 2014). The expression is as follows:

$$F = \sum_{i=1}^{n} \tau_i |A_i| \tag{5}$$

where τ_i is the element shear stress and A_i is the element area of the overflow wall.

The element shear stress τ can be obtained from the following equation:

$$\tau = \tau_\omega + \tau_t = \mu \frac{\partial v_x}{\partial y} + \mu_t \frac{\partial \bar{v}_x}{\partial y} \tag{6}$$

where v_x is the instantaneous velocity of the phase state and $\bar{v}_x$ is the time-averaged velocity of the phase state.

The mixed medium conveyed by the mixing pump is a gas-liquid two-phase flow. Thus, when considering the shear stress, the shear stress of both phases needs to be taken into account. This study only takes the area of 1/10 of the inlet end of the blade as the research object. Fig. 8 is the liquid phase shear stress cloud map of the blade leading edge region of the original model and different schemes under the design flow condition (Q = 100 m^3/h) and the IGVF is 40%. From a), it can be seen that the liquid phase shear stress is mainly concentrated on the leading edge of the blade, and its area is similar to that of the dissipative vortex. This indicates that there is collision and friction between the micelles and the wall inside the dissipative vortex and as a result, the shear stress of the liquid increases relative to the wall surface. The distribution of liquid shear stress in the rest of the cloud diagrams extends from the inlet end of the blade to the flow direction, and the extent of extension increases with the increase of height and pitch. This shows that the bionic waveform structure can inhibit the separation of the mixed medium and strengthen the adhesion of the medium on the suction surface, but it also increases the shear stress of the liquid phase on the suction surface during attachment. The liquid phase shear stress in f) increases significantly along the flow direction in the region near the wheel rim, which also shows that the scheme has a poor ability to inhibit separation in the region of high velocity. Under this condition, the mixed medium and the wall still remain in a detached state.

Under the design flow condition (Q = 100 m^3/h) and the IGVF is 40%, the shear stress distribution in the gas phase shear stress nephogram in Fig. 9 is opposite to the shear stress distribution in the liquid phase shear stress nephogram in Fig. 8. In the region with large liquid phase shear stress, the gas phase shear stress is small; in the region with small liquid phase shear stress, the gas phase shear stress is large. This shows that due to the large extrusion effect of the liquid on the wall surface and the much higher density of the liquid phase than the gas phase, the gas phase is pushed out from the wall surface. It then results in large liquid phase shear stress and small gas phase shear stress here. In the back of the liquid phase shear stress concentration area, the extrusion effect of the liquid relative to the wall surface, and also the displacement effect of the gas phase reduced. Therefore, in this area, the liquid phase and the gas phase are mixed and collided to enhance the friction between the gas and the wall surface, resulting in a large gas phase shear stress.

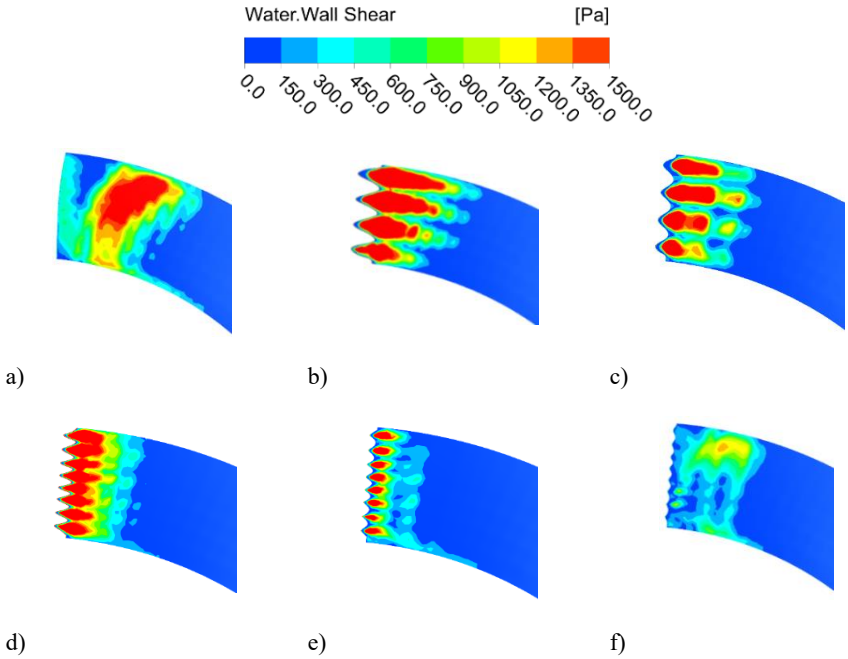

Fig. 8. Liquid phase shear stress in the leading edge area of the suction side: a) original model; b) *A*2*λ*5; c) *A*1*λ*5; d) *A*1*λ*2.5; e) *A*0.5*λ*2.5; f) *A*0.25*λ*2.5.

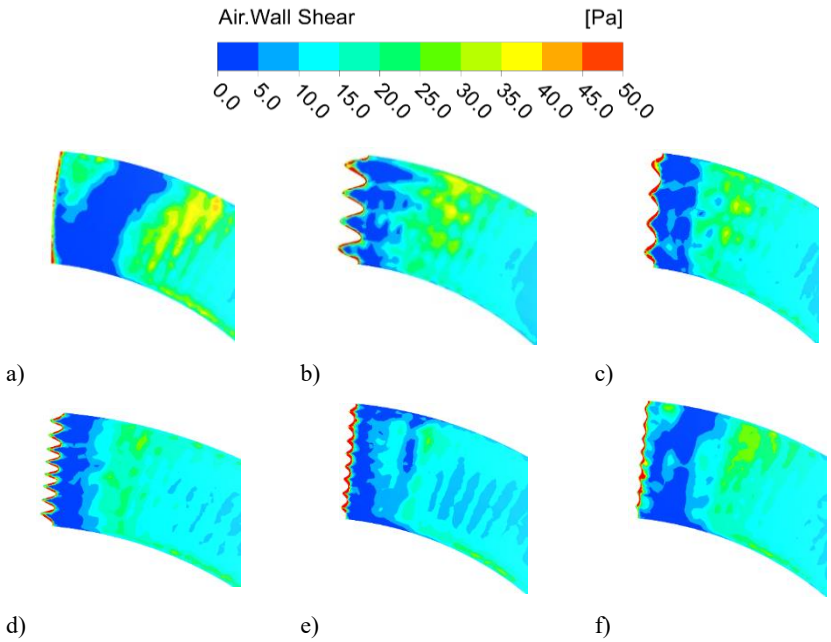

Fig. 9. Gas phase shear stress in the leading edge area of the suction side: a) original model; b) *A*2*λ*5; c) *A*1*λ*5; d) *A*1*λ*2.5; e) *A*0.5*λ*2.5; f) *A*0.25*λ*2.5.

In order to make the original model the same as the selected study area for each scheme, the shear stress at 0.5 times blade height was compared.

Figure 10 shows the liquid and gas phase shear stress curves in the suction front edge region of the original model and different schemes under the design flow condition (Q = 100 m^3/h) and the IGVF is 40%. It can be seen from the figure that the shear stress caused by the two-phase medium of schemes *A*1*λ*5 and *A*1*λ*2.5 on the leading edge of the blade is between schemes *A*2*λ*5 and *A*0.5*λ*2.5. Whether it is the liquid phase shear stress or the gas phase shear stress in the trough region, the bionic corrugated leading edge blade can effectively reduce it. However, at the position of 0.05 times the chord length, the gas-liquid two-phase shear stress of the scheme *A*0.25*λ*2.5 increases, indicating that the mixed medium is separated from the wall again at this position. In general, the ability of the bionic corrugated leading edge blade to suppress the separation of the mixed medium from the wall is much better than the original model. But when the wave height and pitch are too large, the shear stress on the wall increases.

Figure 11 shows the nephogram of the turbulent kinetic energy distribution in the leading edgeregion of the blade in the original model and different schemes under the design flow condition (Q = 100 m^3/h) and the IGVF is 40%. It can be seen from the figure that the turbulent kinetic energy of the original model is mainly concentrated on the leading edge of the blade, and its position corresponds to the position of the dissipative vortex, indicating that there are micelles inside the dissipative vortex, which mix and collide with the wall surface, resulting in an increase in the turbulent kinetic energy of the wall surface. The turbulent kinetic energy distribution in the rest of the cloud images extends from the wave crest along the flow direction, and the extent of extension decreases with decreasing height and pitch, which indicates that the bionic waveform leading edge

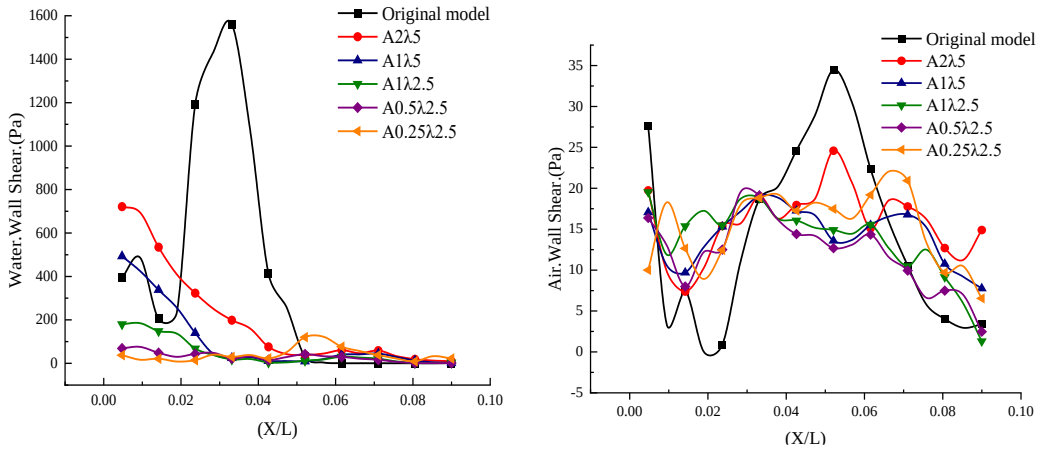

Fig. 10. Liquid and gas phase shear stresses in the leading edge area of the suction side.

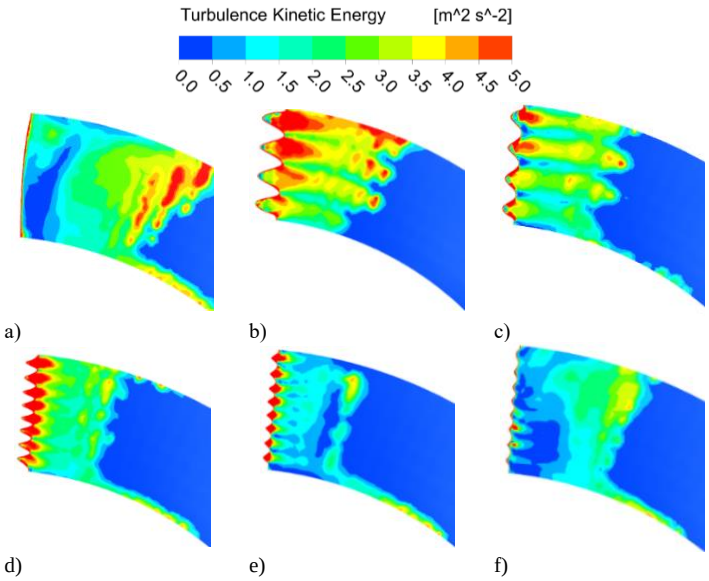

Fig. 11. Turbulent kinetic energy in the leading edge area of the suction side: a) original model; b) *A*2*λ*5; c) *A*1*λ*5; d) *A*1*λ*2.5; e) *A*0.5*λ*2.5; f) *A*0.25*λ*2.5.

blade has the ability to suppress the separation of mixed media and reduce dissipation. However, compared with the original model, the maximum value of the turbulent kinetic energy distribution in f) is significantly reduced, indicating that the scheme has a poor ability to suppress the separation of the medium and the wall in the area of high velocity.

Figure 12 is a graph showing the change of turbulent kinetic energy in the suction side edge region of the blade under the design flow condition (Q = 100 m^3/h) and the IGVF is 40%. It can be seen from the figure that all schemes of the bionic waveform leading edge blade can effectively reduce the turbulent kinetic energy generated by the impact in reducing turbulent kinetic energy. The extreme point of turbulent kinetic energy appears at 0.05 times chord length, indicating that this position is separation between the mixed medium and the wall.

In order more accurately to analyze the variation of shear stress and turbulent kinetic energy data on the suction side of the blade, the average shear stress and average turbulent kinetic energy of the 1/10 region in front of the blade suction side were obtained by averaging the relevant data. The following tables shows the average shear stress and average turbulent kinetic energy of the gas-liquid two-phase mixed medium before and after the modification to the turbulent front 1/10 area of the suction side inlet.

When the gas-liquid two-phase mixed medium enters the impeller, it is impacted by the blades, resulting in the separation of the boundary layer. In addition, the local shear stress and turbulent kinetic energy at the inlet end of the suction surface, as well as the motion resistance of the mixed medium increase. By increasing the pressure difference in the blade height direction at the inlet end of the bionic corrugated blade, the adhesion of the mixed medium to the suction surface is enhanced and the separation is slowed down. The change rates of the gas-liquid two-phase shear stress and turbulent kinetic energy in the table are negative values, which are justified by increased resistance. It can be seen from Tables 3-5 that when the pitch or height is too large, the resistance increases. Under the design flow condition

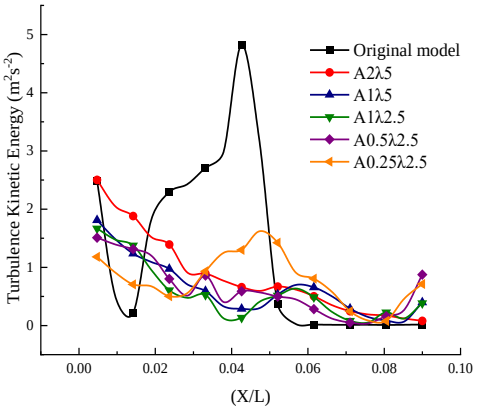

Fig. 12. Turbulent kinetic energy in the leading edge area of the suction side

Table 3 Liquid phase shear stress of different models.

Scheme	Original model (Pa)	Bionic waveform (Pa)	Rate of change (%)
*A*2*λ*5	264.4	525.9	-98.9
*A*1*λ*5	264.4	382.2	-44.5
*A*1*λ*2.5	264.4	282.7	-6.9
*A*0.5*λ*2.5	264.4	178.4	32.5
*A*0.25*λ*2.5	264.4	190.9	27.8

Table 4 Gas phase shear stress of different models.

Scheme	Original model (Pa)	Bionic waveform (Pa)	Rate of change (%)
*A*2*λ*5	13.9	21.2	-52.5
*A*1*λ*5	13.9	24.3	-74.8
*A*1*λ*2.5	13.9	18.0	-29.5
*A*0.5*λ*2.5	13.9	9.9	28.8
*A*0.25*λ*2.5	13.9	12.6	9.4

Table 5 Turbulence kinetic energy of different models.

Scheme	Original model (m^2s^{-2})	Bionic waveform (m^2s^{-2})	Rate of change (%)
*A*2*λ*5	2.6	4.1	-57.7
*A*1*λ*5	2.6	3.1	-19.2
*A*1*λ*2.5	2.6	2.9	-11.5
*A*0.5*λ*2.5	2.6	1.7	34.6
*A*0.25*λ*2.5	2.6	1.9	26.9

(Q = 100 m^3/h) and the IGVF is 40%, in the front 1/10 area of the inlet end of the suction side, the shear stress of the liquid relative to the wall surface is reduced to the maximum by 32.5%, and the shear stress of the gas relative to the wall surface is reduced to the maximum by 28.8%, and the maximum turbulent kinetic energy is reduced by 34.6%.

4.3 Drag Reduction Rate Analysis

The flow resistance of the gas-liquid two-phase mixed medium to the suction surface of the impeller in the mixed pump includes two parts: the shear stress of the medium viscosity on the wall surface and the Reynolds stress of the turbulent state. The calculation formula of the resistance reduction rate is as follows:

$$\eta_0 = \frac{F - F_g}{F} \times 100\% \tag{7}$$

where F is the flow resistance of the mixed medium before modification, and F_g is the flow resistance of the mixed medium after modification.

Figure 13 shows the mixed medium resistance curves of different schemes in the 1/10 area of the inlet end of the suction side of the blade under the design flow condition and different inlet gas contents. It can be seen from the figure that when the pitch is λ = 25%h, the resistance increases. In addition, when the pitch λ = 12.5%h, the drag reduction effect becomes obvious with the decrease in the wave height. However, the scheme *A*0.25*λ*2.5 of the IGVF is 20%~40%, the drag reduction ability decreases. With the continuous increase of IGVF, drag reduction capacity decreases. According to the calculation of the drag reduction rate formula, when the IGVF is 50%, the drag reduction effect of the scheme *A*0.5*λ*2.5 is the best, and the maximum drag reduction rate in the 1/10 area of the inlet end of the blade suction surface is 52.6%. In general, the inlet gas content of the mixed pump and the resistance of the mixed medium show a quadratic function relationship. Besides, with the increase of the inlet gas content, the resistance of the mixed medium shows a downward trend. The relevant fitting

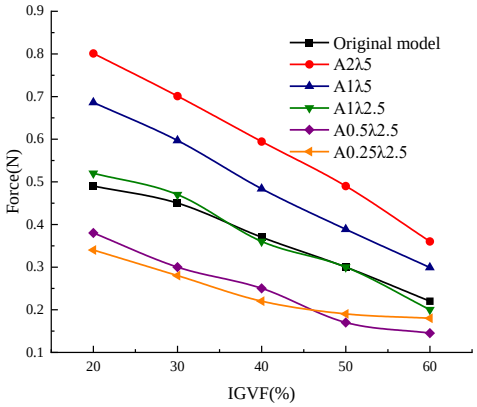

Fig. 13. Mixed medium resistance curve of the front 1/10 area of the inlet end of the blade suction side.

function is as follows:

$$y = ax^2 + bx + c \tag{8}$$

where x is the inlet gas content and y is the resistance of the mixed medium.

The relevant parameter values under different schemes are shown in Table 6.

4.4 Influence of Bionic Waveform Leading Edge Blade on External Characteristics of Mixed Pump

Figure 14 shows the efficiency-head curves of the original model and different modified schemes under the design flow condition and different IGVF conditions. The horizontal axis in the figure represents the IGVF (%) of the mixed pump, and the hollow square curve represents the Efficiency (%) of the left-axis mixed pump, the solid square curve represents the head (m) of the right-shaft mixed pump. From efficiency-head curve, it can be seen that with the increase of the inlet gas content, the efficiency and head of the original model and of the

Table 6 Relevant parameters of the fitting function between inlet gas content and mixed medium resistance.

Scheme	*a*	*b*	*c*
Original model	-5×10^{-5}	-0.0029	0.5720
*A*2*λ*5	-4.11×10^{-5}	-0.0076	0.9687
*A*1*λ*5	1.2×10^{-5}	-0.0109	0.9006
*A*1*λ*2.5	-3.57×10^{-5}	-0.0052	0.6440
*A*0.5*λ*2.5	5.71×10^{-5}	-0.0106	0.5690
*A*0.25*λ*2.5	9.29×10^{-5}	-0.0115	0.5360

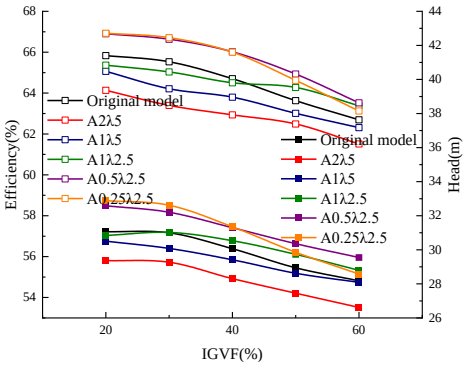

Fig. 14. Efficiency-head curves at different models and at different inlet gas contents.

mixed pump under each scheme show a downward trend. This shows that the main reason for the reduction of the efficiency and head of the mixed pump is the increase of the inlet gas content. The maximum increase in efficiency and head of the mixed pump appears in scheme *A*0.5*λ*2.5. When IGVF is 50%, the efficiency and head of the original model are 63.63% and 28.94m, respectively, while those of scheme *A*0.5*λ*2.5 are 64.93% and 30.35m, respectively. Thus, the maximum increase in efficiency is 2.2% and the maximum increase in head is 4.8%. Comparing *A*2*λ*5 and *A*1*λ*5 schemes at the same pitch, the efficiency and head of the mixed pump are found to be significantly lower than those of the original model. From Tables 3-5, it can be seen that when the height $A \geq 0.5\%L$ and the pitch $\lambda = 25\%h$, the wave front structure increases the adhesion of the mixed medium to the wall surface, resulting in an increase in the flow resistance of the medium. Comparing the same heights in *A*1*λ*5 and *A*1*λ*2.5 schemes, the efficiency curve and head curve of the mixed pump in *A*1*λ*2.5 schemes intersect with the curves of the original model. The efficiency curve of the original model is higher than that of the *A*1*λ*2.5 schemes when the inlet gas content is in the range 20% to 40%. In addition, the efficiency curve of the original model is lower than that of the *A*1*λ*2.5 scheme when the inlet gas content is in range of 40% to 60%. But the efficiency and head in *A*0.5*λ*2.5 and *A*0.25*λ*2.5 schemes are higher than that of the original model. This shows that when the pitch is $\lambda = 12.5\%h$, it is beneficial to reduce the motion resistance of the mixed medium, but when the height $A > 0.5\%L$, the pressure difference in the direction of the wave height will increase, making the adhesion of the medium too large, and the flow resistance increases. Overall, the inlet gas content of the mixed pump has a quadratic function relationship with the efficiency and head. In addition, with the increase of the inlet gas content, the efficiency and head of the mixed pump show a downward trend. The relevant fitting functions are as follows:

$$y = ax^2 + bx + c \tag{9}$$

where x is the inlet gas content and y is the efficiency and head of the mixed pump.

The relevant parameter values under different schemes are shown in Table 7 and Table 8.

5. CONCLUSION

Aiming at the phenomenon that the mixed medium is impacted by the leading edge of the blade and the flow separation occurs, resulting in an increase in the flow resistance, a bionic waveform leading edge blade scheme with different heights *A* and pitches *λ* is proposed. Based on the Fluent solver, numerical calculation is carried out for each scheme of the mixed pump under the design flow condition and the inlet gas content of 20%~60%, and the internal flow characteristics, resistance characteristics and external characteristics of the original model are evaluated. The influence law of the bionic wave leading edge blade on the characteristics of the mixed pump is analyzed and summarized.

Table 7 Relevant parameters of the fitting function between inlet gas content and efficiency.

Scheme	*a*	*b*	*c*
Original model	-1.09×10^{-3}	0.0051	66.2275
*A*2*λ*5	-3.26×10^{-4}	-0.0356	64.8979
*A*1*λ*5	-5.23×10^{-5}	-0.0629	66.2871
*A*1*λ*2.5	-5.88×10^{-4}	-2.1084	65.5769
*A*0.5*λ*2.5	-1.96×10^{-3}	0.0726	66.2348
*A*0.25*λ*2.5	-2.31×10^{-3}	0.0877	66.1234

Table 8 Relevant parameters of the fitting function between inlet gas content and head.

Scheme	*a*	*b*	*c*
Original model	-1.13×10^{-3}	0.0122	31.3874
*A*2*λ*5	-9.77×10^{-4}	0.0049	29.7559
*A*1*λ*5	-2.48×10^{-4}	-0.0431	31.5068
*A*1*λ*2.5	-1.83×10^{-3}	0.0922	29.7739
*A*0.5*λ*2.5	-6.25×10^{-4}	-0.0292	33.4872
*A*0.25*λ*2.5	1.61×10^{-3}	0.0147	33.3572

1) By adjusting the pitch and height of the bionic waveform leading edge blade, the pressure distribution of the leading edge of the blade can be effectively adjusted, and the adhesion of the mixed medium to the wall can be changed. When the height $A > 0.5\%L$ and the pitch $\lambda > 25\%h$, the adhesion of the mixed medium to the suction surface is too large, resulting in increased shear stress and turbulent stress on the wall surface and increased flow resistance. When the height $A = 0.125\%L$, the pitch $\lambda = 12.5\%h$ and the IGVF > 40%, the adhesion of the mixed medium to the suction surface gradually weakens, and the drag reduction ability decreases.

2) When the IGVF of the mixed pump changes, the calculation results under different pitches and heights schemes will vary. When the height $A = 0.25\%L$ and the pitch $\lambda = 12.5\%h$, under the design flow condition and the IGVF is 50%, the drag reduction effect is the best, and the maximum drag reduction in the 1/10 area of the inlet end of the blade suction side is 52.6%, the maximum increase in efficiency is 2.2%, and the maximum increase in head is 4.8%.

ACKNOWLEDGEMENTS

This study was supported by the National Natural Science Foundation of China [Grant no. 52179086]; 52269022; Gansu Provincial Department of Education Project [Grant no. 2021CYZC-27]; the Central Government Guides Local Science and Technology Development Fund Project and Research on Key Technologies for Renovation and Reconstruction of Large Cascade Pump Station in Jingtaichuan Electric Power Irrigation Project.

REFERENCES

Chen, E., C. Wu, A. Yang and G. Li (2021). Numerical study on aerodynamic noise characteristics of sinusoidal leading edge blades. *Fluid Machinery* 49(07), 20-28.

Fonseca, W., R. Silva and R. Orselli (2020). Numerical study of airfoil with wavy leading edge at high Reynolds number regime. *Revista Facultad de Ingeniería* (98).

Gu, Y., J. Mu, D. Dai, S. Zheng, L. Jiang and D. Wu (2015). Drag reduction characteristics of gas-liquid two-phase flow based on gas jet. *Propulsion Technology*.

Guo, C., Z. Zhang, X. Cao, T. Wu and Y. Su (2019). Numerical and experimental studies of hydrodynamic performance of bionic leading-edge tu.bercle airfoil. *Hydrodynamic research and progress* 31(6),10.

Li, F. (2019). Innovative application of multi-phase mixed pump. *Internal Combustion Engine and Accessories* (5),2.

Li, W., Z. Li, Z. Qin, S. Yan, Z. Wang and S. Peng (2022). Influence of the solution pH on the design of a hydro-mechanical magneto-hydraulic sealing device. *Engineering Failure Analysis* 135, 106091.

Li, X. (2020). Influence of blade thickening and distortion law on the performance of spiral axial flow oil-gas mixed pump. *Lanzhou University of* Technology.

Li, Z., W. Li, Q. Wang, R. Xiang, J. Cheng, W. Han and Z. Yan (2021). Effects of medium fluid cavitation on fluctuation characteristics of magnetic fluid seal interface in agricultural centrifugal pump. I*nternational Journal of Agricultural and Biological Engineering* 14(6), 85-92.

Liu, M., L. Tan and S. Cao (2019). Dynamic mode decomposition of gas-liquid flow in a rotodynamic multiphase pump. *Renewable Energy* 139(AUG), 1159-75.

Ma, X., Z. Han, H. Wan and L. Zhang (2021). Influence of changing law of stator vane placement angle on flow characteristics of helical axial-flow mixed pump. *Fluid Machinery* 49(10), 66-73.

Pan, N., S. Zhong and Y. Xu (2016). Research status and progress of oilfield multi-phase mixed transport technology. *Urban Construction Theory Research.*

Rabha, S., M. Schubert, F. Grugel, M. Banowski and U. Hampel (2015). Visualization and quantitative analysis of dispersive mixing by a helical static mixer in upward co-current gas–liquid flow. *Chemical Engineering Journal* 262, 527-40.

Suh, j., Y. Choi, J. Kim, K. Lee and W. Joo (2017). Multiphase flow analysis for air-water bubbly flow in a multiphase pump. In *Fluids Engineering Division Summer Meeting*.

Wang, F. (2020). *Computational Fluid Dynamics Analysis*. Tsinghua University Press.

Wang, G. (2014). Research on flow separation control and application of concave-convex leading edge airfoil imitating whale fin. *Graduate School of Chinese Academy of Sciences*.

Wu, C., E. Chen, A. Yang and G. Li (2021). Numerical analysis of application of bionic blade to centrifugal fan. *Journal of Power Engineering* 41(4), 8.

Wu, J. (1986). The incompressible theory of interaction between moving objects and vorticity field—the generation and dissipation of vorticity field on the object surface. *Journal of Aerodynamics* (2), 44-52.

Wu, Z., X. Hao, R. Rong and S. Wang (2014). Research on drag reduction mechanism of ridged surface airfoil blades. *Journal of System Simulation* 26(6), 7.

Yu, F., A. Ren and K. Liu (2004). Research statue of helical axial-flow pump for multiphase transfer. *Oil Field Equipment*.

Zhang. J., S. Cai, Y. Li, H. Zhu and Y. Zhang (2016). Visualization study of gas–liquid two-phase flow patterns inside a three-stage rotodynamic multiphase pump. *Experimental Thermal & Fluid Science* 70, 125-138.

Zhang, Z. and W. Li (2020). Research on the aerodynamic characteristics of the leading edge of the pectoral fin bionic blade of a humpback whale. *Engineering Mechanics*.

Zhao, B., L. Han, Y. Liu, W. Liao, Y. Fu and Z. Huang (2022). Influence of blade Placement Angle of mixed flow pump on internal vortex structure and adaptability of impeller and guide vane. *Journal of Drainage and Irrigation Machinery Engineering* 40(2), 109-114.

Zhao, M., Y. Zhao and Z. Liu (2020). Dynamic mode decomposition analysis of flow characteristics of an airfoil with leading edge protuberances. *Aerospace Science and Technology*.

Zhou, C. (2021). Influence of airfoil leading edge Sag and trailing edge uptilt on performance of helical axial flow gas-liquid Mixed Pump. *Lanzhou University of Technology*.